ELSEVIER

Journal of Hazardous Materials A:64 (1999) 223–247

Journal of Hazardous Materials

The representation of dynamic flow effects in a Lagrangian puff dispersion model

R.I. Sykes *, C.P. Cerasoli, D.S. Henn

ARAP Group, Titan Research and Technology, 50 Washington Road, P.O. Box 2229, Princeton, NJ 08543-2229, USA

Received 12 August 1998; revised 2 December 1998; accepted 9 December 1998

Abstract

A technique for incorporating buoyancy-driven dynamics in a Lagrangian puff model is described. The dynamic effects are non-linear and therefore proper treatment requires interaction integrals for overlapping puffs. Conservation laws for the volume integral of momentum and buoyancy over an individual puff are based on the fundamental equations of motion. A simplified representation of the field of motion associated with the buoyancy-driven dynamics is then used to move and distort the puffs. The effects associated with dense gas 'slumping' on the ground are represented by lateral divergence of the velocity field, with a magnitude based on conservation of the moment of vorticity. The model predictions are compared with a number of experimental results on buoyant plume rise and dense gas dispersion.

Keywords: Atmospheric dispersion; Plume rise; Dense gas effects; Lagrangian puff

1. Introduction

Many pollutant releases into the atmosphere involve dynamic flow effects associated with differences in temperature and/or density. One example is the elevated stack source, where hot gases are emitted as a vertical jet and form a buoyant plume. The buoyant rise is important since it can strongly influence the effective release height and

* Corresponding author. Tel.: +1-609-452-2950; fax: +1-609-452-2856; e-mail: isykes@titan.com

0304-3894/99/$ - see front matter
PII: S0304-3894(98)00271-4

source size for the subsequent atmospheric dispersion. However, buoyancy effects can be positive or negative. Volatile materials stored under pressure will form a dense cloud when accidentally released due to cooling associated with the latent heat of vaporization. Many gases used in industrial processes may have molecular weights larger than air and are denser than air even at ambient temperatures. In proximity to the ground, a dense cloud will tend to spread laterally, and the vertical diffusion will be suppressed. This can give rise to high ground-level concentrations, so the prediction of dense gas dispersion in the atmosphere is a topic of considerable interest for emergency response and site safety studies.

The rise of a hot, positively buoyant plume is often prescribed as part of the initial conditions for the dispersion calculation using analytical expressions such as those in Ref. [2]. However, the transition to a passive dispersion code requires an arbitrary choice for the position at which the dynamics can be neglected. Furthermore, the rise phase may extend a significant distance downstream from the source location and the plume concentrations may be required during this period. The Briggs formulae are also restricted to relatively idealized situations, and do not strictly address factors such as time-dependent releases or multiple interacting plumes. A more general description within the Lagrangian puff framework can provide this increased capability.

A number of models currently exist for predicting the evolution of negatively buoyant dense gas releases in the atmosphere. Ref. [5] reviewed a selection of these models and compared their predictions with a set of experimental observations. The models generally fall into three categories: Navier–Stokes codes, puff/plume codes and analytic formulae. The puff/plume models are generally accepted as being the most practical, since Navier–Stokes codes are too complex and more appropriate for research studies, while closed analytic formulae are too limited in their application. Within the puff/plume category, there is a distinction between a continuous release, where a steady-state plume model is used, and the instantaneous release of a single puff. Transient releases are sometimes modeled as a finite length section of a plume, but the models do not properly describe complex effects such as multiple source interactions. As in the buoyant rise case, a full Lagrangian puff description can provide a more general capability.

The difficulty in representing dynamic effects in a general Lagrangian puff model arises from the non-linear character of the phenomena. The puff approach [1] is based on the linearity of the advection–diffusion equation, which describes the dispersion of a passive tracer and allows the concentration field to be formed from the superposition of independent Lagrangian puffs. However, in the presence of buoyancy-driven dynamics, the motion of one part of the concentration field cannot be calculated without regard for the rest of the distribution. The dynamic representation therefore requires an interaction calculation, so that each puff is influenced by the dynamic properties of other puffs. A similar interaction requirement is demanded for the representation of the concentration fluctuation variance, since this is a non-linear quantity, and this has been addressed in the SCIPUFF model described in Ref. [13]. The puff interaction computation in SCIPUFF (Second-order Closure Integrated Puff) therefore provides a framework for including non-linear dynamic effects. In the following sections, we describe the puff representation of these dynamic motions, and illustrate the model predictions for a range of test flows.

2. Puff model description

2.1. Mean flow variables

SCIPUFF uses a Gaussian puff representation to describe the concentration field as the sum of contributions from a collection of puffs. A three-dimensional Gaussian is completely described by its spatial integral moments up to second-order and can be written in the form

$$c(x) = \frac{Q}{(2\pi)^{3/2}(\mathrm{Det}(\sigma))^{1/2}} \exp\left[-\frac{1}{2}\sigma_{ij}^{-1}(x_i - \bar{x}_i)(x_j - \bar{x}_j) \right]. \tag{1}$$

Note that we use a generalized tensor definition of the moments to describe shear distortions, as described in Ref. [10].

Using an angle bracket to denote an integral over all space, the spatial moments in Eq. (1) are defined as

Zeroth moment—mass

$$Q = \langle c \rangle \tag{2}$$

First moment—centroid

$$Q\bar{x}_i = \langle c x_i \rangle \tag{3}$$

Second moment—spread

$$Q\sigma_{ij} = \langle c(x_i - \bar{x}_i)(x_j - \bar{x}_j) \rangle \tag{4}$$

Evolution equations for these moments can be derived from the advection–diffusion equation, and involve turbulent fluctuation correlations. A turbulence closure model for the fluctuation terms due to ambient atmospheric turbulence, appropriate for a passive tracer release, is described in Refs. [11,13]. The puff moment equations for a passive tracer are included in Appendix A. Dynamical effects due to puff buoyancy require extension to the passive tracer model, and we now discuss the methodology.

Buoyancy dynamics requires the storage of additional variables for each puff. The model for positively buoyant releases is based on the conservation equations for buoyancy, $\langle \bar{\theta}_p \rangle$, and vertical momentum, $\langle \bar{w}_p \rangle$, where θ is the potential temperature, w is the vertical velocity and the subscript p denotes the dynamic puff perturbation from the local ambient atmospheric value.

The evolution of the mean dynamic variables is based on the Boussinesq momentum equation and the conservation of potential temperature, giving

$$\frac{\mathrm{d}}{\mathrm{d}t}\langle \bar{w}_p \rangle = \frac{g}{T_0}\langle \bar{\theta}_p \rangle \tag{5}$$

$$\frac{\mathrm{d}}{\mathrm{d}t}\langle \bar{\theta}_p \rangle = -\frac{\partial \theta_B}{\partial z}\langle \bar{w}_p \rangle \tag{6}$$

where θ_B is the ambient potential temperature. These equations neglect the pressure gradient in the momentum equation, and simply represent the buoyant acceleration term in Eq. (5) and the change in buoyancy due to vertical motion through a potential temperature gradient in Eq. (6).

The mean dynamic variables in Eqs. (5) and (6) determine the equilibrium rise of a buoyant puff in a stable atmosphere, where the ambient temperature gradient is inverted (i.e. positive), but the solution will oscillate indefinitely about the equilibrium level. The vertical velocity itself will be damped, due to turbulent entrainment which increases the effective volume of the integrals, but the integrated momentum and buoyancy will be undamped. While the buoyancy is strictly conserved, the integrated vertical momentum will actually be reduced due to the generation of gravity waves, and the oscillation will be damped. This effect is represented by a simple linear damping on the vertical velocity integral, so that Eq. (5) becomes

$$\frac{\mathrm{d}}{\mathrm{d}t}\langle \overline{w}_p \rangle = -\frac{g}{T_0}\langle \overline{\theta}_p \rangle - c_w N \langle \overline{w}_p \rangle \tag{7}$$

where N is the Brunt–Vaisala frequency and $c_w = 0.1$. N is only defined non-zero for stable temperature gradients and a damping coefficient of 0.1 is chosen to provide a reasonably rapid adjustment to the equilibrium height.

Tracking the independent evolution of the dynamics of each puff is not sufficient, however, to model the buoyant rise effects since these effects are interactive. A plume of positively buoyant gas rises differently from an isolated buoyant puff because the flow field induced by the buoyancy has an influence on other parts of the plume. These effects are represented by means of correlation integrals for the momentum and buoyancy, which account for turbulent fluctuations in addition to the non-linear interactions. The correlation equations are written as

$$\frac{\mathrm{d}}{\mathrm{d}t}\langle \overline{w_p c} \rangle = -\frac{g}{T_0}\langle \overline{\theta_p c} \rangle - c_w N \langle \overline{w_p c} \rangle - \frac{\langle \overline{w_p' c'} \rangle}{\tau_c} \tag{8}$$

$$\frac{\mathrm{d}}{\mathrm{d}t}\langle \overline{\theta_p c} \rangle = -\frac{\partial \theta_B}{\partial z}\langle \overline{w_p c} \rangle - \frac{\langle \overline{\theta_p' c'} \rangle}{\tau_c} \tag{9}$$

where τ_c is the fluctuation dissipation timescale [13] which must be modified to account for the dynamically-induced turbulence. The turbulence model will be described below.

Note that the turbulent dissipation terms, the last terms in Eqs. (8) and (9), involve the fluctuation correlations, which are defined as

$$\langle \overline{w_p' c'} \rangle = \langle \overline{w_p c} \rangle - \langle \overline{w}_p \bar{c} \rangle$$

$$\langle \overline{\theta_p' c'} \rangle = \langle \overline{\theta_p c} \rangle - \langle \overline{\theta}_p \bar{c} \rangle$$

The mean overlap integrals, $\langle \overline{w}_p \bar{c} \rangle$ and $\langle \overline{\theta}_p \bar{c} \rangle$, are calculated in a manner similar to the mean concentration overlap terms, $\langle \bar{c}^2 \rangle$, as described in Ref. [13]. This effectively assumes the same Gaussian distribution for both vertical velocity and potential temperature. Thus, we estimate

$$\langle \overline{\theta}_p \bar{c} \rangle^{(\alpha)} = Q^{(\alpha)} \sum_{\beta} \langle \overline{\theta}_p \rangle^{(\beta)} \langle G^{(\alpha)}(x) G^{(\beta)}(x) \rangle \tag{10}$$

where the superscripts denote puffs numbered α and β, and $G^{(\alpha)}(\boldsymbol{x})$ is the Gaussian shape function for puff-α defined in Eq. (1). The summation in Eq. (10) is taken over all puffs and multiplies the temperature field due to puff-β by the concentration field due to puff-α. This could result in n^2 overlap terms for a calculation with n puffs, but SCIPUFF eliminates unnecessary calculations using an efficient scheme to determine which interaction pairs are significant. Overlapping puffs are also merged together, so that the total number of puffs is minimized [10].

The dynamic correlations provide an additional vertical velocity component, which is added to the ambient velocity field used to transport the puff centroid. Thus, the equation for the vertical component of the centroid location becomes

$$\frac{\mathrm{d}\bar{z}}{\mathrm{d}t} = \overline{w}(\bar{x}) + \hat{w}_{\mathrm{p}} \tag{11}$$

where $\overline{w}$ is the ambient vertical velocity and the dynamic rise velocity is given by

$$\hat{w}_{\mathrm{p}} = \frac{\langle \overline{w_{\mathrm{p}} c} \rangle}{Q}. \tag{12}$$

We note that the model only represents the vertical component of the internal puff momentum, so that the rise can be calculated. The horizontal velocity is not perturbed from the ambient wind field.

2.2. Buoyant gas representation

Buoyancy effects can arise directly from a density difference between the ambient air and the gas material. This is particularly important for dense gas effects, discussed in the Section 2.4, but is introduced here for the simpler case of buoyant rise. If the gas is lighter than air, then it will tend to rise without any temperature perturbation. In this case, the buoyancy variable is actually

$$g\left(\frac{\theta}{T_0} - m\frac{\Delta\rho}{\rho_0}\right)$$

where m is the mass mixing ratio, ρ_0 is the ambient air density and $\Delta\rho$ is the density difference $\rho_{\mathrm{gas}} - \rho_0$. Since the local species concentration value, c, is equal to $m\rho_{\mathrm{gas}}$, we can define the total gas buoyancy as

$$b = \frac{\theta}{T_0} - \frac{c\Delta\rho}{\rho_{\mathrm{gas}}\,\rho_0}.$$

In order to treat non-Boussinesq density perturbations associated with very dense gases, we modify the gravity term so that the effective acceleration due to the gas density difference cannot exceed g. The correction factor of $1 + b$ in the denominator is only applied for positive density perturbations, since lighter-than-air materials must still accelerate the surrounding air mass, sometimes known as the added mass effect.

The dynamic puff integral equations are thus modified to give

$$\frac{\mathrm{d}}{\mathrm{d}t}\langle \overline{w}_{\mathrm{p}} \rangle = \frac{g\langle \overline{b}_{\mathrm{p}} \rangle}{1+\hat{b}} - c_w N \langle \overline{w}_{\mathrm{p}} \rangle \tag{13}$$

for the buoyant gas puffs, and

$$\frac{\mathrm{d}}{\mathrm{d}t}\langle \overline{w_{\mathrm{p}} c} \rangle = \frac{g\langle \overline{b_{\mathrm{p}} c} \rangle}{1+\hat{b}} - c_w N \langle \overline{w_{\mathrm{p}} c} \rangle - \frac{\langle \overline{w'_{\mathrm{p}} c'} \rangle}{\tau_c} \tag{14}$$

$$\frac{\mathrm{d}}{\mathrm{d}t}\langle \overline{b_{\mathrm{p}} c} \rangle = -\frac{\langle \overline{b'_{\mathrm{p}} c'} \rangle}{\tau_c} \tag{15}$$

for all puffs. The non-Boussinesq density correction is defined as

$$\hat{b} = \max\left(0, \frac{\langle \overline{b_{\mathrm{p}} c} \rangle}{\langle \overline{c} \rangle}\right) \tag{16}$$

Note that the buoyancy correlation term is simply damped toward the mean overlap value, which is computed in the same way as the temperature overlap.

2.3. Turbulent entrainment

The velocity field induced by the dynamic rise of a cloud is turbulent and the ambient diffusion is enhanced by the internal turbulence of the cloud. The additional entrainment and dissipation is modeled using an estimate of the internal turbulent velocity and length scales. The entrainment model is based on earlier work on power plant plume rise [12] and relates the turbulent velocity to the vertical rise rate. We define

$$q_{\mathrm{p}}^2 = F_{\mathrm{p}}(\mathrm{Ri}_{\mathrm{p}})\hat{w}_{\mathrm{p}}^2\left(c_{\mathrm{q}1} + c_{\mathrm{q}2}\frac{V^2}{V^2+\hat{w}_{\mathrm{p}}^2}\right). \tag{17}$$

The entrainment factor contains a term that depends on the ambient wind speed, V, which models the increased entrainment in a bent-over plume due to the vortex pair formation. The stability factor

$$F_{\mathrm{p}} = 1 + 4\mathrm{Ri}_{\mathrm{p}} \tag{18}$$

represents the increased turbulent energy production due to buoyancy-driven instabilities. The puff Richardson number is defined as

$$\mathrm{Ri}_{\mathrm{p}} = \frac{g\Lambda_{\mathrm{p}}|\hat{b}_{\mathrm{p}}|}{\hat{w}_{\mathrm{p}}^2} \tag{19}$$

where Λ_{p} is the length scale of the internal turbulence. The dynamic buoyancy variable is defined similarly to the dynamic vertical velocity as

$$\hat{b}_{\mathrm{p}} = \frac{\langle \overline{b_{\mathrm{p}} c} \rangle}{Q}.$$

The dynamic length scale, Λ_p, is defined equal to the concentration fluctuation length scale, Λ_c [13], since this represents an instantaneous scale for the dispersing cloud. The empirical coefficients in Eq. (17) are chosen as $c_{q1} = 0.4$ and $c_{q2} = 3.0$ from fitting jet rise data, as discussed below. Additionally, an upper limit of 2 is imposed on F_p to prevent excessive entrainment velocities.

The dynamic velocity and length scales are used to define a dynamic diffusivity, which is added to the spatial moment equations (see Appendix A) to give

$$\frac{d\sigma_{ij}}{dt} = \sigma_{ik}\frac{\partial \bar{u}_j}{\partial x_k} + \sigma_{jk}\frac{\partial \bar{u}_i}{\partial x_k} + \frac{\langle x_i' \overline{u_j' c'} \rangle}{Q} + \frac{\langle x_j' \overline{u_i' c'} \rangle}{Q} + 2K_p\delta_{ij} \tag{20}$$

where

$$K_p = 0.15 q_p \Lambda_p. \tag{21}$$

The dynamic turbulence also modifies the rate equations for the internal length scales, so that we obtain

$$\frac{d\Lambda_c}{dt} = q_c^{amb} + 0.15 q_p \tag{22}$$

where the first term accounts for the ambient turbulence [13]. An additional term is also included in the fluctuation dissipation timescale, τ_c, to account for the internally generated turbulence. Since the length scale for the dynamic turbulence is already assumed to be equal to the instantaneous fluctuation scale, the additional term is simply proportional to the effective energy dissipation time scale.

2.4. Dense gas dynamics

The puff treatment of buoyancy-driven dynamics described in Section 2.3 must be modified for the description of negatively buoyant dense gas dispersion. The most important feature of dense gas dynamics is the interaction with the solid ground surface, which causes lateral spreading as the dense cloud collapses and suppresses the vertical diffusion due to the stable density distribution. We first address the dynamic spreading effect, where the gravitational forcing term drives motion parallel to the ground instead of a vertical acceleration. The gravitational force is still directed vertically, but the lateral motion is induced by the pressure gradient, which was ignored in the buoyant rise situation. We therefore require a treatment of the equations of motion that include the surface-induced pressure gradient.

A convenient starting point for modeling the dynamics is the vorticity equation, obtained by taking the curl of the momentum equation,

$$\frac{\partial \omega_i}{\partial t} + u_j\frac{\partial \omega_i}{\partial x_j} = \omega_j\frac{\partial u_i}{\partial x_j} + \varepsilon_{ijk} g_j \frac{\partial b}{\partial x_k} + \nu\frac{\partial^2 \omega_i}{\partial x_j \partial x_j} \tag{23}$$

where $\omega = \nabla \times u$ is the vorticity, ν is the kinematic viscosity and the buoyancy forcing is written in the same form as in Section 2.3. Note that the pressure gradient term is absent in this formulation. Forming the vertical component of the vorticity moment

$$P = \boldsymbol{e}_3 \cdot (x \times \omega)$$

where $\boldsymbol{e}_3$ is the unit vector in the vertical direction, and integrating over all space, we obtain

$$\frac{\mathrm{d}}{\mathrm{d}t}\langle P\rangle = g\langle \bar{b}_{\mathrm{p}}\rangle + S_P \tag{24}$$

where S_P represents a surface integral term. Ignoring the surface term for the moment, it is evident that P is very closely related to the vertical momentum integral in Section 2.3. In fact, far from a solid boundary, $\langle P\rangle$ satisfies exactly the same evolution equation as $\langle \overline{w}_{\mathrm{p}}\rangle$ and can therefore be identified as the integrated vertical momentum.

In order to use Eq. (24) as a basis for the dense gas puff dynamics, we must represent the surface integral term and relate puff motions to the vorticity moment integral. Since the velocity field strictly vanishes at a solid boundary, the surface integral S_P involves only the viscous diffusion terms; we therefore represent it as a drag term, whose detailed specification will be described below. The relationship between the vorticity moment integral and the puff dynamics is based on a simple shape assumption for the induced velocity field, since the relation between velocity and vorticity is linear. This allows us to superpose the velocity fields from neighboring puffs by simple addition and represent the interactions between a collection of dense puffs. The vorticity moment evolution Eq. (24) also depends linearly on the buoyancy integral, so that summing the moments of individual puffs can also represent the total vorticity moment. The puff evolution is still non-linear as the dynamic fields are composed of the summation over all puffs, but the puff moments evolve independently and the basis of the dynamics is contained in the shape assumption for the velocity field.

In general, the velocity field induced by a dense gas cloud involves an outward radial flux in the cloud itself, spreading the material horizontally over the ground surface. This horizontal divergence is accompanied by a vertical velocity gradient as material moves downward toward the ground. A schematic cross-section is illustrated in Fig. 1. This flow field is associated with azimuthal vorticity and we can obtain a general relation between the velocity magnitude and the vorticity moment.

If we assume that the magnitude of the horizontal radial velocity is U_0, the radial dimension is L_{H}, and the vertical dimension is L_{V}, then the vorticity magnitude will be

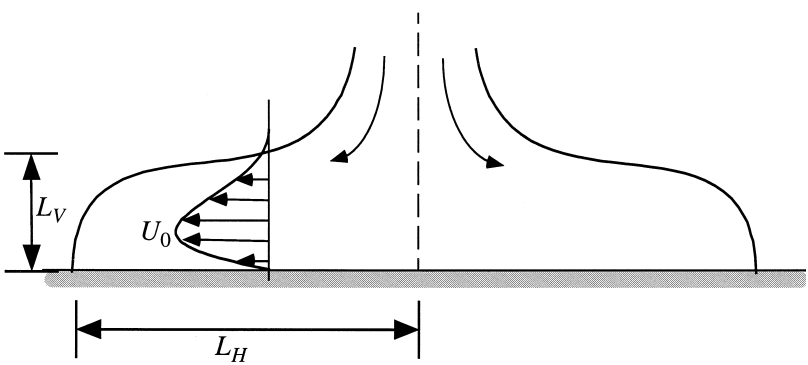

Fig. 1. Schematic illustration of slumping dense cloud.

U_0/L_V. This neglects the horizontal gradient of the vertical velocity component in the definition of vorticity, but this contribution is negligible when the cloud is shallow in comparison with its width. An order of magnitude estimate for the vorticity moment is thus obtained as $U_0 L_H^3$, using L_H as the magnitude of the radial vector, $\boldsymbol{x}$, and $L_H^2 L_V$ as the volume estimate.

A simple assumption for the radial velocity field uses the Gaussian form to give

$$u_r = U_0 \frac{r}{L_H} \exp\left(- \frac{r^2}{L_H^2} \right). \tag{25}$$

This satisfies the linear gradient requirement at the center of the puff and vanishes at large distances. We cannot assume circular symmetry since SCIPUFF uses a generalized Gaussian description and the velocity shape assumption must be applied to elliptical puffs. As an asymptotic condition, we consider the extreme case where the ellipse becomes an infinite line and require that the spreading velocity be directed transverse to the line. Using this condition to define the limiting behavior, the radial distribution given in Eq. (25) can be generalized to an elliptical shape as

$$\begin{aligned} u_X &= U_0 \frac{X}{L_X} \frac{L_Y}{L_H} \exp\left(- \frac{X^2}{L_X^2} - \frac{Y^2}{L_Y^2} \right) \\ u_Y &= U_0 \frac{Y}{L_Y} \frac{L_X}{L_H} \exp\left(- \frac{X^2}{L_X^2} - \frac{Y^2}{L_Y^2} \right) \end{aligned} \tag{26}$$

where X and Y are the principal coordinates in the horizontal plane for an elliptical puff, with the puff centroid as origin, and $2L_H^2 = L_X^2 + L_Y^2$. The length scales, L_X and L_Y, are related to the semi-major axes of the puff as

$$L_{X,Y} = C_{d1} \left(\frac{\sigma_{xx} + \sigma_{yy}}{2} \pm \frac{1}{2} \sqrt{(\sigma_{xx} - \sigma_{yy})^2 + 4\sigma_{xy}^2} \right) \tag{27}$$

and the empirical coefficient C_{d1} is chosen to be 1.5. Note that the velocity components in Eq. (26) must be rotated from the frame of the principal axes into the (x,y) calculation coordinates. Horizontal velocity gradients are computed by differentiating Eq. (26) and rotating the four components appropriately. In principal axes coordinates, the velocity gradients are

$$\begin{aligned} \frac{\partial u_X}{\partial X} &= \left(1 - 2\frac{X^2}{L_X^2} \right) \frac{U_0}{L_X} \frac{L_Y}{L_H} \exp\left(- \frac{X^2}{L_X^2} - \frac{Y^2}{L_Y^2} \right) \\ \frac{\partial u_Y}{\partial Y} &= \left(1 - 2\frac{Y^2}{L_Y^2} \right) \frac{U_0}{L_Y} \frac{L_X}{L_H} \exp\left(- \frac{X^2}{L_X^2} - \frac{Y^2}{L_Y^2} \right) \\ \frac{\partial u_X}{\partial Y} &= -2XY \frac{U_0}{L_H} \exp\left(- \frac{X^2}{L_X^2} - \frac{Y^2}{L_Y^2} \right) \\ \frac{\partial u_Y}{\partial X} &= -2XY \frac{U_0}{L_H} \exp\left(- \frac{X^2}{L_X^2} - \frac{Y^2}{L_Y^2} \right). \end{aligned} \tag{28}$$

The scaling velocity, U_0, is related to the vorticity moment, which we identify with $\langle \overline{w}_p \rangle$. Integrating the moment of the vorticity based on vertical gradients of the velocity field, we obtain

$$U_0 = -\frac{\langle \overline{w}_p \rangle}{\pi} \frac{L_H}{L_X^2 L_Y^2}. \tag{29}$$

Specification of the individual puff velocity field leads to the evolution equations for the puff moments, using both velocity and velocity gradients. These quantities are calculated at the puff centroid location by summing the contributions from all the overlapping puffs. Note that a single puff has zero mean velocity at its centroid, since the components in Eq. (26) vanish when $X = Y = 0$, but the two diagonal gradients in Eq. (28) are non-zero, so the puff is stretched in the horizontal plane.

The dynamically induced velocity and velocity gradients are simply added to the ambient flow field to produce the total transport and distortion of the puffs. The vertical velocity gradient is defined from the sum of the two horizontal divergence components, maintaining a total divergence of zero. The vertical component of velocity is defined from the velocity gradient, assuming zero as the surface boundary condition. Thus,

$$\frac{\partial w_d}{\partial z} = -\left(\frac{\partial u_d}{\partial x} + \frac{\partial v_d}{\partial y} \right) \tag{30}$$

where the subscript d denotes the overlap sum from all contributing puffs with dense dynamics. The vertical velocity of the centroid is defined as

$$w_d = \bar{z} \frac{\partial w_d}{\partial z} \exp\left(-\frac{\bar{z}}{\Lambda_{cV}} \right) \tag{31}$$

where $\bar{z}$ is the puff centroid height. Λ_{cV} is a representative vertical scale height for the puff and satisfies a similar equation to the internal puff scale, Λ_c, in Eq. (22). The 'slumping effect' is manifested through the inclusion of the vertical velocity gradient, given by Eq. (30), in the equations for both the vertical spread, σ_{zz}, and the vertical scale, Λ_{cV}. The exponential decay factor in Eq. (31) is introduced to limit the descent velocity for puffs further from the surface. The horizontal stretching motion for a single puff is thus associated with a vertical compression and downward motion of the centroid.

The dense gas effects are only calculated for puffs that interact with the ground surface. Negatively buoyant puffs remote from the surface will simply fall downward under the buoyancy forcing described in Section 2.1. Puffs are judged to interact with the ground when they have negative vertical momentum, $\langle \overline{w_p c} \rangle$, and their centroid is less than $2\Lambda_{cV}$ above the ground. The first requirement ensures that they are descending and the second checks that they are in contact with the ground. When these conditions are satisfied, the ambient temperature gradient term in the buoyancy correlation equations, Eqs. (6) and (9), is neglected, since the vertical velocity integral is interpreted as a vorticity moment and there is no vertical transport at the solid surface.

The model for the 'slumping' velocity presented above may seem much more complicated than the representation used in existing dense gas dispersion models such as

HGSYSTEM [15]. Most simple models calculate the horizontal spread velocity from a pseudo-balance between the kinetic energy of the horizontal motion and the potential energy associated with the density perturbation, using the simple relation

$$u_{\text{slump}} \propto \sqrt{gH\frac{\rho - \rho_{\text{a}}}{\rho}} \tag{32}$$

where H is the cloud depth, ρ is the cloud density and ρ_{a} is the ambient density. This relationship is not derived from the momentum conservation equations, however, and is not readily generalized to describe the effects from overlapping puffs. Under simplified conditions, the more fundamental model given by Eqs. (25)–(29) can be shown to predict similar behavior to Eq. (32). In particular, if we neglect all turbulent entrainment and assume small density perturbations, it can be seen that

$$\frac{\mathrm{d}}{\mathrm{d}t}\langle \overline{w}_{\text{p}} \rangle = g\langle \overline{b}_{\text{p}} \rangle \tag{33}$$

and

$$\frac{\mathrm{d}}{\mathrm{d}t}\langle \overline{b}_{\text{p}} \rangle = 0 \tag{34}$$

i.e. the total buoyancy is conserved and the vertical momentum, or vorticity moment, increases linearly with time. For a circular puff, the spreading velocity scale is given by

$$U_0 = -\frac{\langle \overline{w}_{\text{p}} \rangle}{\pi L_{\text{H}}^3} \tag{35}$$

and the lateral scale L_{H} thus increases according to

$$\frac{\mathrm{d}L_{\text{H}}}{\mathrm{d}t} \propto U_0 \propto \frac{t}{L_{\text{H}}^3} \tag{36}$$

giving a growth of the lateral scale proportional to $t^{1/2}$, consistent with the simple model prediction. For a 'line' puff, with $L_X \gg L_Y$, we have

$$\frac{\partial u_X}{\partial X} \cong 0$$

$$\frac{\partial u_Y}{\partial Y} \cong \frac{U_0}{L_Y} \tag{37}$$

and

$$U_0 = \frac{\langle \overline{w}_{\text{p}} \rangle}{\pi L_X L_Y^2}. \tag{38}$$

The volume integral will be proportional to the 'line' length, L_X, so the effective spread velocity will be inversely proportional to L_Y^2. The results in a lateral spread proportional to $t^{2/3}$, again consistent with simple model predictions for a line source.

2.5. Dense gas effects on turbulent entrainment

The presence of the ground introduces stability effects on the turbulence in addition to the pressure gradient effects of the mean velocity field. In a free atmosphere, any density perturbation forms a stable vertical gradient on one side and unstable on the other. A free dense cloud is unstable on the lower side, while a positively buoyant perturbation is unstable on the upper side. However, when the density perturbation is constrained by the ground surface, a stable gradient is established throughout the cloud. The density gradient suppresses vertical turbulent diffusion since vertical motions transfer kinetic energy to potential energy as the density perturbations are mixed. This mechanism applies to the ambient turbulent motions as well as the dynamically induced motions in the slumping dense cloud.

When a puff is determined to interact with the ground, as given above, a dense cloud turbulence entrainment model is applied. The framework is similar to the buoyant rise parameterization in Section 2.3, but we use the following velocity and length scales appropriate for a stably stratified dense cloud.

The internal velocity scale for a dense gas puff is based on the lateral velocity since vertical motion is constrained. Similarly, the length scale is based on the vertical scale of the cloud as the turbulent eddies are also constrained by the solid boundary. The internal turbulent velocity scale is given by

$$q_d^2 = c_{q1} F_d^2(\mathrm{Ri}_d) V_d^2 \tag{39}$$

where

$$V_d^2 = u_d^2 + v_d^2 + (\sigma_{xx} + \sigma_{yy}) \left(\frac{\partial w_d}{\partial z} \right)^2 \tag{40}$$

$$F_d = \frac{1}{1 + C_{d2} \mathrm{Ri}_d} \tag{41}$$

and

$$\mathrm{Ri}_d = \frac{g \Lambda_d |\hat{\theta}_p / T_0 - \hat{b}_p|}{V_d^2 + V^2}. \tag{42}$$

The dynamic velocity scale V_d represents the 'slumping' motion in the dense cloud. The gradient term is required to provide the velocity scale for the self-induced motions in a puff, since the mean self-induced velocity Eq. (26) is zero at the puff centroid. The internal dynamic scale, Λ_d, is taken to be the vertical puff scale, Λ_{cV}, since the vertical cloud depth characterizes the shear-generation scale. The Richardson number is based on the total velocity, because the effective stability is determined by the balance between buoyancy and shear and ambient motions are included in this balance. The coefficient in Eq. (41), C_{d2}, is chosen to be 25 on the basis of comparisons with laboratory data.

In addition to the stability effect on the internally generated turbulence, the formation of a stable layer at the ground affects the ambient turbulence and mean velocity profile. Boundary layer turbulence is principally driven by interaction with the ground surface,

and the reduction of vertical transport through the dense cloud layer can significantly modify the local profiles. We represent this effect by applying the damping factor F_d to the ambient vertical eddy diffusivity, $\langle z'\overline{w'c'}\rangle/Q$, as defined in Appendix A The distortion of the mean ambient velocity profile is represented by reducing the puff centroid velocity by a factor $0.7 + 0.3F_d$. This follows the suggestion in Ref. [7] based on field experiments with significant density effects.

The turbulent diffusivity, dissipation timescale and internal horizontal scale equation are modified as in Eqs. (21) and (22), but using q_d and Λ_d in place of q_p and Λ_p.

2.6. Surface drag

As the dense cloud moves over the ground surface, the frictional drag of the rough surface tends to reduce the lateral slumping rate. This effect is represented by the surface integral terms in Eq. (24). We represent the drag effect through a damping coefficient on the vertical momentum (or vorticity moment) integrals, $\langle \overline{w}_p \rangle$ (or $\langle P \rangle$) and $\langle \overline{w_p c}\rangle$. In addition, the interaction with the ground introduces a heat flux directly into the cloud and we assume that this exchange rate occurs at the same rate as the momentum exchange. The damping is therefore applied also to the temperature perturbation integrals.

The surface time scale is based on the roughness length, z_0, and a logarithmic wall-layer assumption. An inverse time scale is defined as

$$\tau_w^{-1} = \frac{1}{u_b}\frac{\partial u_b}{\partial t} \tag{43}$$

and we assume that

$$\frac{\partial u_b}{\partial t} = \frac{\partial \tau}{\partial z}$$

where τ is the turbulent momentum flux. We then use the cloud height scale and the wall-layer relation between the surface stress and local wind speed to obtain

$$\tau_w^{-1} = \left(\kappa \Big/ \log\left(1 + \frac{\Lambda_d}{z_0}\right)\right)^2 \frac{\sqrt{V^2 + V_d^2}}{\Lambda_d}. \tag{44}$$

3. Buoyant rise test calculations

The vertical rise dynamics in SCIPUFF have been tested principally against idealized laboratory experiments or in comparison with well-accepted empirical relations based on laboratory and field experiments. These include momentum jets in a cross-flow, and buoyant plumes in neutral or stable temperature gradients with a crossflow.

3.1. Momentum jet

The first experiments considered are momentum jets (no buoyancy) in a crossflow. Ref. [4] (from Ref. [6]) presents near-source data for a variety of exit velocity ratios, $R = W_0/U_a$, where U_a is the crossflow velocity and W_0 is the jet exit velocity. The jet source in SCIPUFF is characterized by a momentum flux F_m and Gaussian spread σ_0, so that W_0 is estimated by assuming an initially uniform velocity distribution such that $W_0^2 = F_m/r_0^2$, where r_0 is the source radius. We also assume that $\sigma_0 = r_0$. A comparison with the mean jet centerline data of Gordier is shown in Fig. 2. SCIPUFF tends to under-predict the jet heights; this is particularly so near the source, but the discrepancies tend to decrease with downstream distance. The high R data show much less downstream displacement of the jet close to source; this is probably due to distortion of the background flow, a phenomenon not included in the SCIPUFF model.

The asymptotic behavior of the momentum jet far downstream is also of interest and here we compare SCIPUFF with the well-known expression (see Refs. [14] or [2])

$$\frac{z'}{\ell_m} = \left(\frac{3}{\beta^2}\right)^{1/3} \left(\frac{x}{\ell_m}\right)^{1/3} \tag{45}$$

where x is downstream distance, z' is the jet centerline height above the source, β is an empirical entrainment constant typically set to 0.6, and the momentum length scale

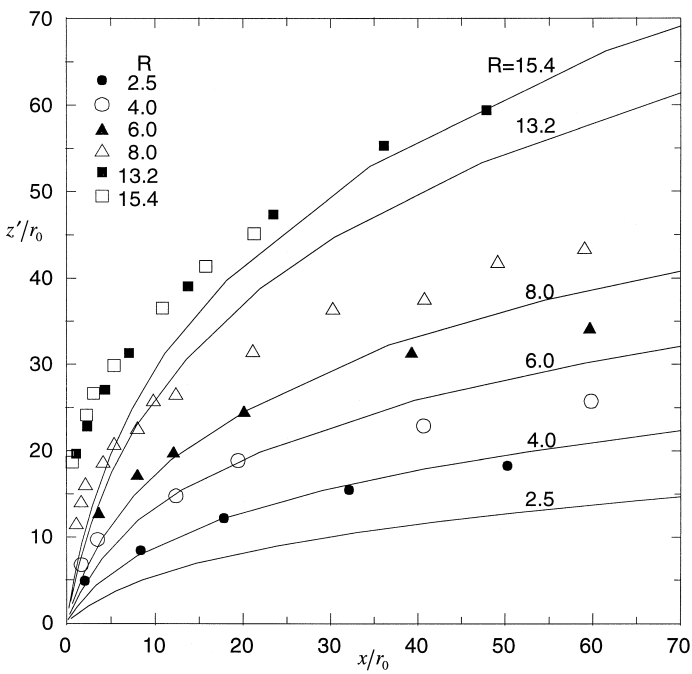

Fig. 2. Momentum (non-buoyant) jet centerline height, z', as a function of downstream distance for a range of R. Symbols are the data in Ref. [4] (from Ref. [6]), solid lines are the SCIPUFF predictions.

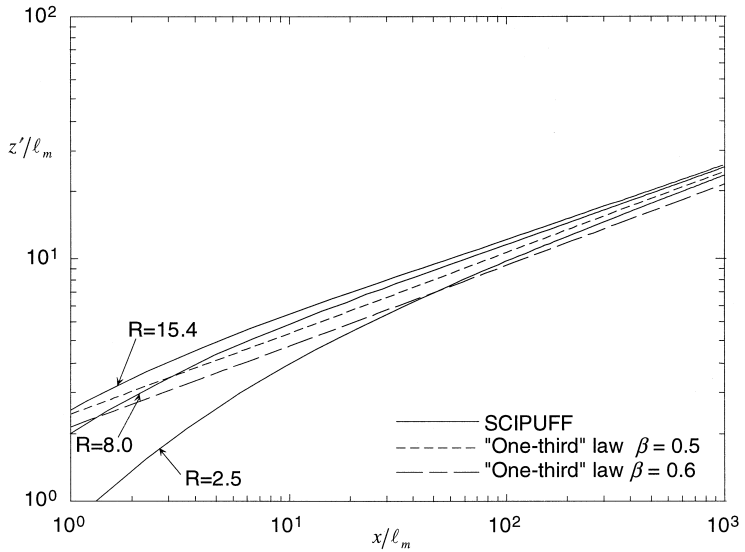

Fig. 3. Comparison between SCIPUFF predictions of momentum jet centerline heights for a range of R (solid lines) and the 'one-third' law, (45), with two values of β (short dashes, $\beta = 0.6$; long dashes, $\beta = 0.5$).

$\ell_m = Rr_0$. Fig. 3 shows the SCIPUFF calculations for three velocity ratios compared with Eq. (45). It can be seen that while there is naturally some initial dependence on R, the three cases show the same asymptotic behavior. The model predictions are consistent with the one-third power law but indicate a value for β around 0.5.

3.2. Buoyant plume

For a buoyancy-dominated plume in a neutral background, the plume height is given by the 'two-thirds' power law [2]:

$$\frac{z'}{\ell_b} = \left(\frac{3}{2\beta^2}\right)^{1/3} \left(\frac{x}{\ell_b}\right)^{2/3} \tag{46}$$

where the buoyancy length scale is given by $\ell_b = F_b/U_a^3$. The buoyancy flux, F_b, is defined as $F_b = W_0 r_0^2 g \Delta T_0/T_a$ where ΔT_0 is the source temperature perturbation relative to the ambient temperature T_a. The 'two-thirds' law has been shown to compare well with numerous field and laboratory data [2]. The 'one-third' and 'two-thirds' laws are essentially limiting cases of a more general expression [14]. Thus, for plumes with significant buoyancy and momentum fluxes, the trajectory is given by

$$\frac{z'}{\ell_b} = \left[\frac{3}{\beta^2}\left(\frac{\ell_m}{\ell_b}\right)^2 \frac{x}{\ell_b} + \frac{3}{2\beta^2}\left(\frac{x}{\ell_b}\right)^2\right]^{1/3} \tag{47}$$

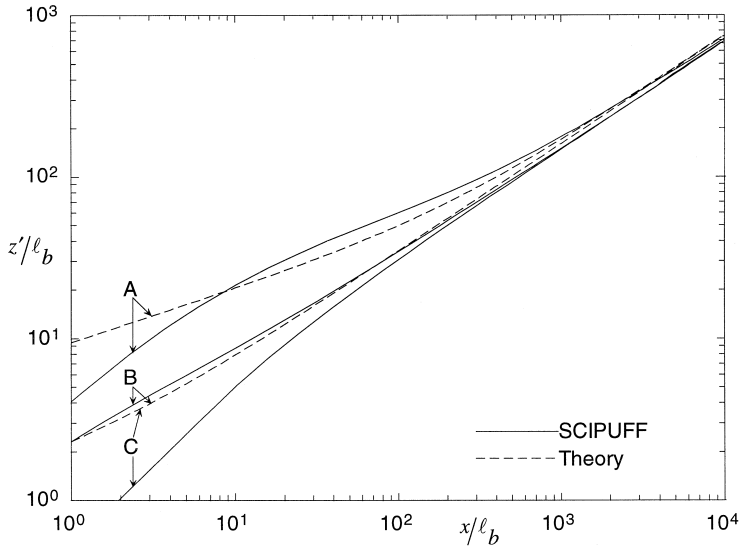

Fig. 4. Comparison between SCIPUFF predictions for buoyancy-dominated jet centerline heights (solid lines) and theory given by Eq. (47) (dashed lines). (Case A) $R = 10$, $F_b^2/U_a^4 F_m = 0.01$; (Case B) $R = 10$, $F_b^2/U_a^4 = 1$; (Case C) $R = 1$, $F_b^2/U_a^4 F_m = 1$.

which reduces to Eq. (46) for $x \gg \ell_m^2/\ell_b$ and to Eq. (45) with $x \ll \ell_m^2/\ell_b$. A comparison of Eq. (47) with the SCIPUFF predictions for a range of buoyancy fluxes

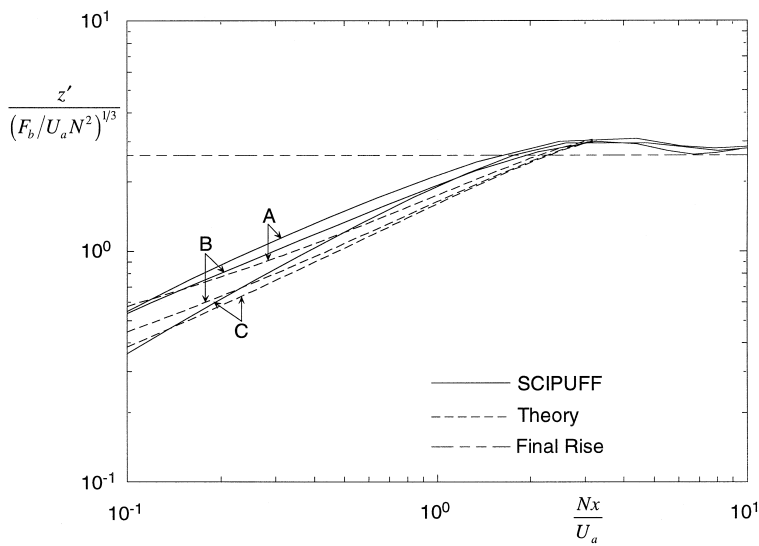

Fig. 5. Comparison of SCIPUFF buoyancy-dominated jet centerline heights in a uniformly stratified background (solid lines) with (48) and (49) (dashed lines). For all cases, $R = 10$. (Case A) $F_b^2/U_a^4 F_m = 0.01$, $F_b N/U_a^4 = 0.00572$; (Case B) $F_b^2/U_a^4 F_m = 1$, $F_b N/U_a^4 = 0.00572$; (Case C) $F_b^2/U_a^4 F_m = 1$, $F_b N/U_a^4 = 0.181$.

and source sizes is shown in Fig. 4. As expected, there are some discrepancies near the source, but the agreement with the two-thirds law is excellent further downstream.

Plume rise in a uniformly stratified environment (N^2 = a positive constant) has been investigated in Ref. [2] which gives the following expression, which accounting for the 'added mass' due to the displacement of ambient fluid by the plume:

$$\frac{z'}{\left(F_b/U_a N'^2\right)^{1/3}} = \left(\frac{3}{\beta'^2}\right)^{1/3}\left(N'\frac{F_m}{F_b}\sin\frac{N'x}{U_a} + 1 - \cos\frac{N'x}{U_a}\right)^{1/3} \tag{48}$$

for $N'x/U_a \le \pi$ where $N' = N/(1+k_v)^{1/2}$, $\beta' = \beta/(1+k_v)^{1/2}$ and k_v is the added mass coefficient (set to 1, the value for a circular cylinder). Based on an extensive survey of field and laboratory data, Ref. [2] also determined an empirical expression for the 'final' plume rise in stable air as

$$z'_{\text{final}} = 2.6\left(F_b/U_a N^2\right)^{1/3}. \tag{49}$$

The SCIPUFF predictions for a range of buoyancy fluxes and stability gradients compare favorably with Eqs. (48) and (49), as shown in Fig. 5.

4. Dense gas test calculations

4.1. Laboratory data comparisons

Preliminary calculations were made with the dense gas model to determine the empirical coefficients used to set the horizontal length scale for the velocity field and the Richardson number damping factor.

The simplest test flow is the collapse of a volume of dense gas in still air. Ref. [8] reports on a laboratory study of this idealized case and their data have been utilized to define the empirical coefficients in SCIPUFF. The second laboratory experiment used to define model coefficients is the wind-tunnel study in Ref. [3], where a continuous plume of dense gas was released into a neutral boundary layer.

Fig. 6 shows the comparison between the model predictions and the data in Ref. [8]. The figure shows concentration vs. time for three near-surface sampler locations at non-dimensional distances of 2.6, 5.8 and 9.2 from the center of an initial cloud of volume 54 l and density ratio 2.90. Results from three independent experiments are shown, illustrating the variability in the instantaneous concentration field. The radial distance is made non-dimensional using the cube root of the initial volume, which is a cylinder with height equal to the diameter. The important features of the comparison are the arrival time of the gas at the various samplers, which is largely controlled by the velocity spread coefficient C_{d1} in Eq. (27) and the magnitude of the concentration, which is controlled by the damping coefficient, C_{d2}. The model predictions are clearly much smoother than the observed concentration time history, as expected for an ensemble average prediction. The initial peak in the concentration, most noticeable at the closest sampling location, is due to the rolling vortex at the leading edge of the density current. This feature is not represented by the integrated puff equations with the

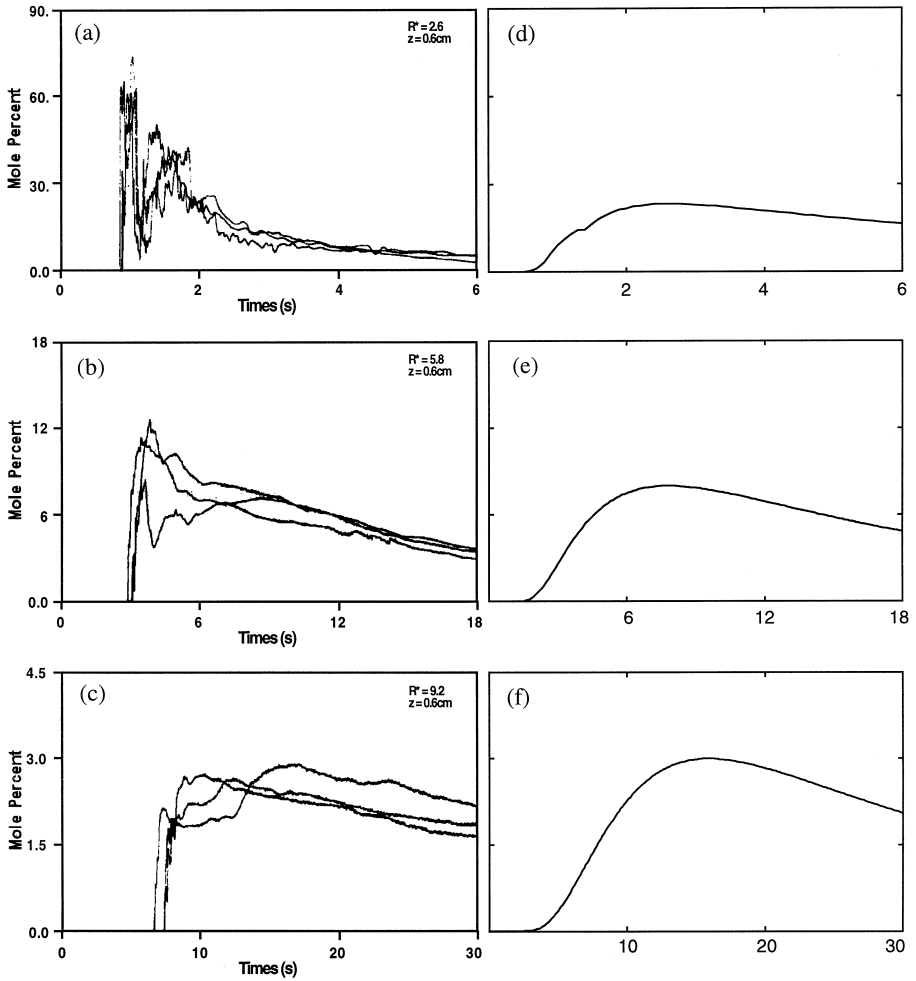

Fig. 6. Comparison between SCIPUFF prediction and the laboratory data in Ref. [8]. Measurements of the concentration time history at $z = 0.6$ cm from three realizations are shown for non-dimensional distances of (a) 2.6, (b) 5.8, (c) 9.2; the ensemble average model predictions are shown at the same locations in (d), (e) and (f), respectively.

Gaussian shape assumption, but is also subject to significant random variability so that the peak would be reduced in a true ensemble average. The arrival time of the main cloud and the magnitude of the concentration at the three samplers are reasonably represented by the puff calculation.

Figs. 7 and 8 show horizontal and vertical profiles from Ref. [3] compared with the SCIPUFF predictions at two downstream locations. Measured velocity and turbulence profiles were used to define the flow field for the dispersion calculation. The figures show the differences between a passive release and a dense release of CO_2 with a density of about 1.5 times that of ambient air. The model predictions show reasonable

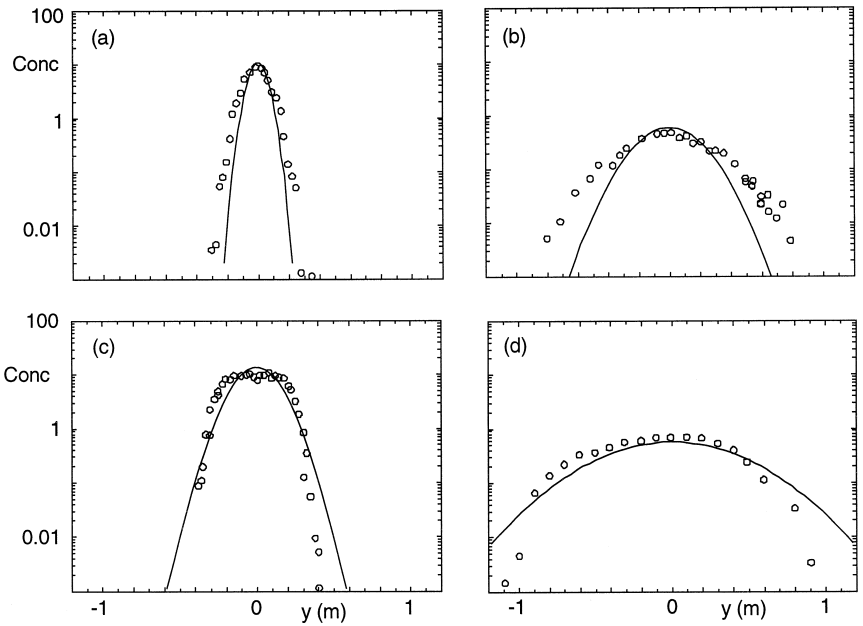

Fig. 7. Horizontal plume cross-sections at ground level. Data points are from Ref. [3]. Solid line is model prediction. (a) neutral release at $x = 0.6$ m, (b) neutral release at $x = 5$ m, (c) dense release at $x = 0.6$ m, (d) dense release at $x = 5$ m.

agreement with the data and illustrate the effect of the gas density. The dense gas results show a wider plume than the passive case and a restricted vertical diffusion. There is good agreement for concentration values above 10% of the surface value for the near source location. However, the shape of the measured profile is not Gaussian. Since the shallow plume near the source is represented by a single Gaussian puff in the vertical direction, SCIPUFF does not match the experiment at the higher positions. At the downstream location, the puffs have split vertically and provide a much better description of the profile shape. The initial profiles would be better described by a different shape function, and this could be implemented for surface-based puffs, but we note that the Gaussian assumption does provide a good description for the higher concentration values.

4.2. Field data comparisons

The Model Data Archive (MDA), compiled by Sigma Research, is an extensive collection of field experiment data for both dense and passive tracer gas releases. The data set contains both continuous and instantaneous sources with different sampling times and has been used to evaluate a number of existing atmospheric dispersion models [5]. Using the model coefficients defined from the preliminary test calculations, SCIPUFF has been compared with the test cases in the Model Data Archive (MDA).

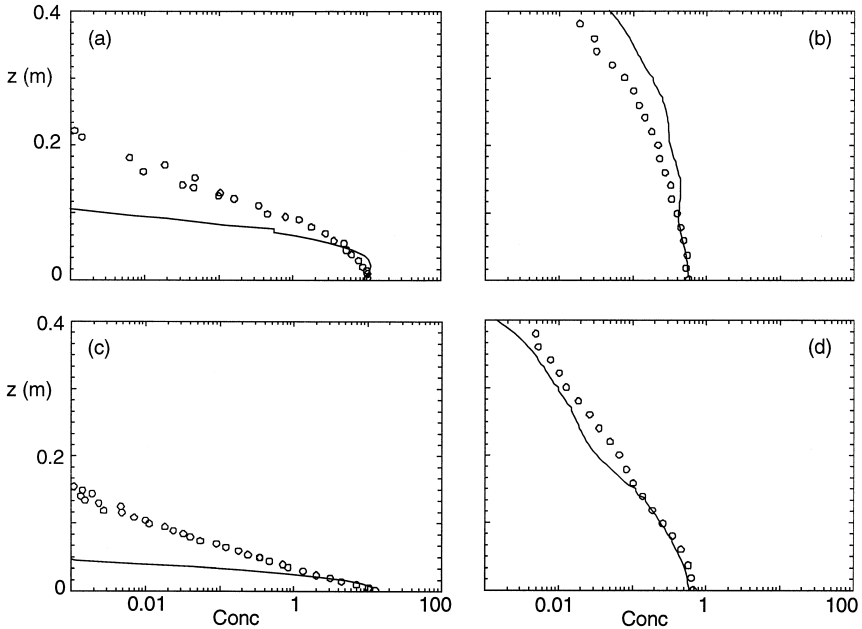

Fig. 8. Vertical plume cross-sections. Data points are from Ref. [3]. Solid line is model prediction. (a) neutral release at $x = 0.6$ m, (b) neutral release at $x = 5$ m, (c) dense release at $x = 0.6$ m, (d) dense release at $x = 5$ m.

The experimental data are divided into a passive release set and a dense gas release set. The passive releases are relatively straightforward, since the only source parameters are the mass flow rate and the source size. The initial standard deviation of the puffs is set equal to the source radius for these releases, which include the Prairie Grass and Hanford data. The dense releases are for evaporating pools, and we use a lateral standard deviation of 75% of the specified pool radius and a vertical standard deviation of 0.5 m for all cases. The vertical size is chosen arbitrarily to represent a typical vertical growth during transport across the pool, and results are not sensitive to the precise value. The initial buoyancy flux was determined from the given mass flux and the difference between the gas boiling temperature and the ambient value. We assume that the vaporizing material is released at the boiling point, so the buoyancy flux is

$$F_B = \frac{Q(T_b - T_a)c_p^{(gas)}}{\rho_{air} c_p^{(air)}} \tag{50}$$

where c_p is the specific heat, T_b is the boiling point, T_a is the air temperature, and Q is the mass flow rate. The dense gas releases include the Maplin Sands, Burro and Coyote tests.

Two special cases were the Desert Tortoise and Goldfish releases, since they involve a two-phase aerosol and exothermic reaction with the environment. SCIPUFF does not contain a model for aerosol evaporation and the thermodynamics of the reactions were not prescribed. A simple linear expansion model was used to estimate the distance to

complete evaporation, and the initial buoyancy flux was then based on the total latent heat transfer.

Whenever possible, the meteorology for the dispersion calculation was specified using a surface heat flux estimate. Many of the data sets include an estimate of the Monin–Obukhov length, which is equivalent to a heat flux specification if the surface friction velocity is known. All cases include a wind speed at a reference height and Pasquill stability category was used only when the heat flux was unavailable. Mean velocity profiles were prescribed using surface layer similarity and turbulence profiles were based on the friction velocity and heat flux.

The data specifies an averaging time for the concentration data and both short and long duration averages are included. The measurements provide the maximum recorded concentration, over all sampling locations at a given distance and over the sampling period. For the long duration measurements, which usually correspond to the release duration, the model is run with the sampling period, T_{avg}, as the appropriate averaging time for filtering the turbulence, and the centerline maximum prediction is used for comparison. For the short duration data, we use the statistical SCIPUFF prediction to estimate the expected value. When a short duration peak, say a 1-s average, is reported from a number of samplers over a sampling period, T_{sample}, it must be recognized that this peak value is a random variable. For an idealized continuous release of infinite duration, we expect the maximum observed value to increase as the sampling period increases, since there is a higher probability of measuring an extreme value. In order to model the expected peak value, we use the predicted probability distribution for the centerline concentration, c_0, using a turbulence filter timescale of T_{avg}. If only one measurement (in time) of the maximum concentration over a number of sampler locations across the plume is made, then the expected value would be $\bar{c}_0$. However, if we sample for a longer time, then the expected peak value must increase since the chances of encountering a higher value are increased.

Suppose that the probability density function for c_0 is such that

$$\text{Prob}(c_0 < X) = P_0(X).$$

Then, if the maximum from N independent observations of c_0 is denoted as c_N, then

$$\text{Prob}(c_N < X) = P_N(X) = \left[P_0(X)\right]^N$$

since all N observations must be less than X. If we can estimate N, therefore, we can determine the expected value of c_N as the predicted value for the observed maximum concentration. We estimate N from the behavior of the concentration fluctuation variance with averaging time, which is reduced by a factor of

$$\frac{2}{\beta^2}\left(\beta - 1 + \mathrm{e}^{-\beta}\right)$$

where $\beta = T_{\text{sample}}/T_{\text{c}}$ and T_{c} is the integral timescale of the fluctuations [9]. If we identify this reduction with the factor $1/N$ for the variance reduction from averaging N independent samples of a discrete variable, then we obtain

$$N^{-1} = \frac{2}{\beta^2}\left(\beta - 1 + e^{-\beta}\right). \tag{51}$$

The calculation procedure, therefore, is:

(a) reduce $\overline{c'^2}$ to account for the averaging time, T_{avg};
(b) determine the clipped normal distribution $P_0(X)$ for the reduced variance;
(c) determine the exponent N from Eq. (51);
(d) calculate the expected maximum value from the distribution P_N.

Results for the overall comparison are shown in Fig. 9, for the passive, and Fig. 10, for the dense gas data sets. The overall agreement with the range of data is relatively good and shows better performance for the passive releases than the dense cases. There is evidence of a slight under-prediction in the dense results, particularly for the lower concentration levels further downstream. Unfortunately, the data do not provide sufficient information to determine the cause of the under-prediction, which may be in the source specification, the lateral slumping representation or the vertical mixing rate. The overall performance is comparable with the best of the existing models. Most of the predictions are within a factor of 2 of the observations and there is reasonable skill in predicting the effect of time averaging on the maximum concentration.

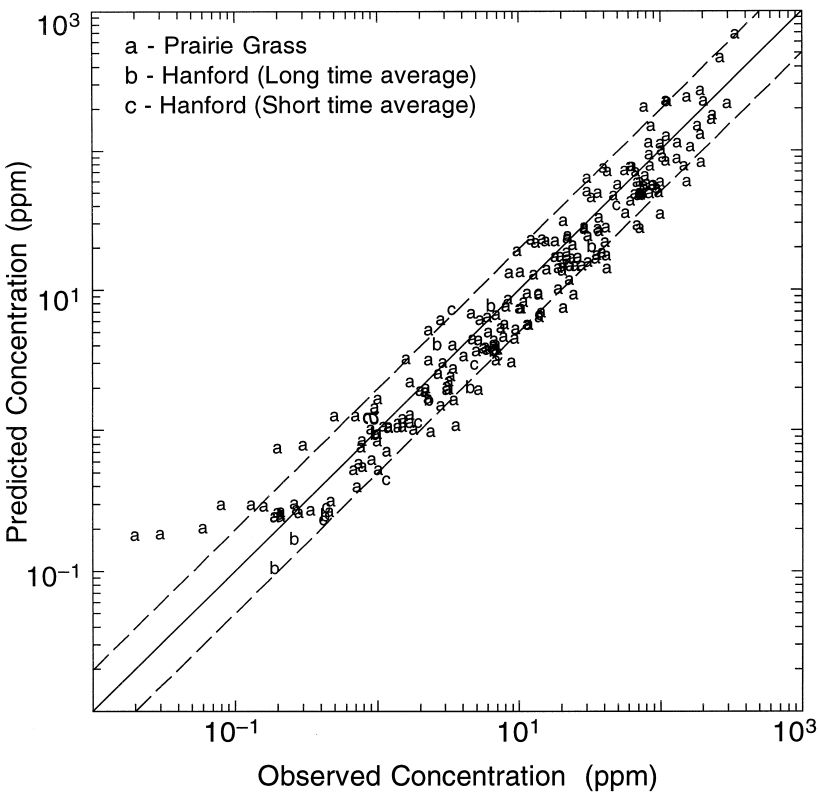

Fig. 9. Scatter plots for SCIPUFF predictions of the MDA passive release data sets.

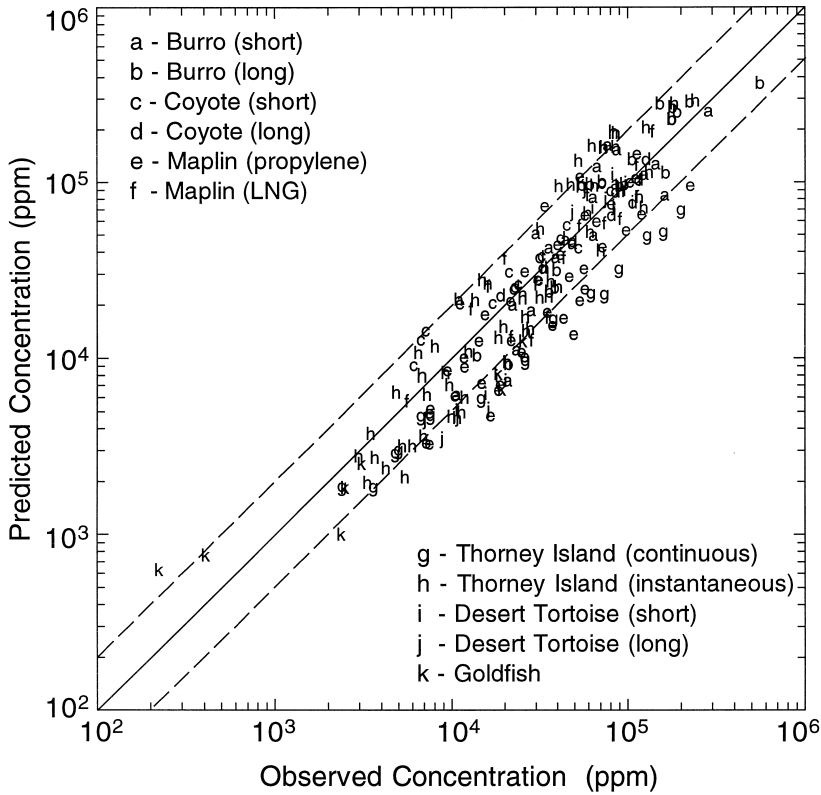

Fig. 10. Scatter plots for SCIPUFF predictions of the MDA dense gas release data sets.

Table 1 presents the geometric mean and variance measures defined in Ref. [5]. The geometric bias is defined as

$$\mathrm{MG} = \exp\left(\frac{1}{N}\Sigma(\ln M - \ln P)\right)$$

and the geometric variance as

$$\mathrm{VG} = \exp\left(\frac{1}{N}\Sigma(\ln M - \ln P)^2\right)$$

where P is the predicted and M the measured value. N is the number of measured values in the data set.

Table 1
Performance measures for the MDA test cases

Data sets	N	MG	VG
Dense cases	217	1.06	1.33
Passive cases	244	1.00	1.31

5. Conclusion

A methodology has been described for including dynamic effects in a Lagrangian puff model. The technique can represent buoyant rise of a puff or plume and can also describe dense gas effects. The interaction between puffs is accounted for by an overlap integral, which provides a general model for arbitrary sources. Finite duration effects or general unsteady sources can be modeled, in addition to multiple sources.

Buoyant rise is modeled using the vertical momentum integral to provide a rise velocity. The effects of turbulent entrainment and a stable ambient atmosphere are also included. Dense gas effects are particularly complicated, since the interaction with the ground prevents a simple vertical motion, and induces lateral spreading. A vorticity moment representation is used to obtain integral equations for the puff and a simple shape function relates the dynamic velocity field to the moments.

The model requires a small number of empirical coefficients, which have been chosen to fit experimental data. The puff conservation equations are based on momentum and buoyancy conservation and are consequently able to reproduce the proper dependence on external parameters such as wind speed, stability gradients and source fluxes. Quantitative agreement with observational data is then obtained by adjusting the empirical constants in the puff equations. The SCIPUFF predictions have been compared with a reasonably wide range of observations, covering plume rise due to buoyancy and momentum, and also a number of dense gas dispersion experiments.

Acknowledgements

This work was supported by the US Defense Special Weapons Agency under contract number DNA001-95-C-0180.

Appendix A. Puff moment equations

A brief description of the evolution equations for the puff variables in the absence of dynamic effects is included here. A more complete discussion can be found in Ref. [13].

Using the mass conservation equation, the equations for the moments defined in Eqs. (2)–(4) are derived as

$$\frac{\mathrm{d}Q}{\mathrm{d}t} = 0 \tag{A1}$$

$$\frac{\mathrm{d}\bar{x}_i}{\mathrm{d}t} = \bar{u}_i(\bar{x}) \tag{A2}$$

$$\frac{\mathrm{d}\sigma_{ij}}{\mathrm{d}t} = \sigma_{ik}\frac{\partial \bar{u}_j}{\partial x_k} + \sigma_{jk}\frac{\partial \bar{u}_i}{\partial x_k} + \frac{\langle x_i' \overline{u_j' c'} \rangle}{Q} + \frac{\langle x_j' \overline{u_i' c'} \rangle}{Q}. \tag{A3}$$

The overbar denotes the ensemble average and fluctuations from the mean are denoted by a prime. Conservation of total mass is expressed by Eq. (A1), while Eq. (A2) moves the centroid with the mean wind. Turbulent diffusion is represented by the fluctuation correlation terms in Eq. (A3) and this equation also accounts for the effect of velocity gradients on the puff spread (see Ref. [10]).

This completes the specification of the puff moment equations, but we have introduced turbulent flux moments in Eq. (A3). The turbulent fluctuations are modeled empirically using turbulence closure techniques as described in Refs. [11,13]. The equation for the moment of the lateral velocity correlation is

$$\frac{\mathrm{d}}{\mathrm{d}t}\langle y'\overline{v'c'}\rangle = Q\overline{v'^2} - A\frac{q}{\Lambda}\langle y'\overline{v'c'}\rangle \tag{A4}$$

where $\overline{v'^2}$ is the variance of the lateral velocity component, q is the total r.m.s. velocity fluctuation, Λ is the turbulence length scale and A is an empirical closure constant. The vertical correlation moment satisfies a similar equation, but includes buoyancy terms.

References

[1] A. Bass, Modelling long range transport and diffusion, Second Joint Conf. on Appl. of Air Poll. Met., AMS and APCA, New Orleans, LA, 1980, pp. 193–215.

[2] G.A. Briggs, Plume rise predictions, in: D.A. Haugen (Ed.), Lectures on Air Pollution and Environmental Impact Analysis, Am. Met. Soc., Boston, MA, 1975, pp. 59–111.

[3] R.E. Britter, W.H. Snyder, Fluid modeling of dense gas dispersion over a ramp, J. Haz. Mat. 18 (1988) 37–67.

[4] R.L. Gordier, Studies on fluid jets discharging normally into moving liquid, St. Anthony Falls Hyd. Lab., University of Minnesota, Vol. 28, Series B, 1959.

[5] S.R. Hanna, J.C. Chang, D.G. Strimaitis, Hazardous gas model evaluation with field observations, Atmos. Environ. 27A (1993) 2265–2285.

[6] E.A. Hirst, Analysis of round, turbulent, buoyant jets discharged to flowing stratified ambients, Oak Ridge National Laboratory, ORNL-4685, 1971.

[7] J.S. Puttock, A model for gravity-dominated dispersion of dense-gas clouds, in: J.S. Puttock (Ed.), Stably Stratified Flows and Dense Gas Dispersion, Clarendon Press, Oxford, 1988.

[8] T.O. Spicer, J.A. Havens, Modeling the phase I Thorney Island experiments, in: J. McQuaid (Ed.), Heavy Gas Dispersion Trials at Thorney Island, Elsevier, Oxford, 1985.

[9] R.I. Sykes, The variance in time-averaged samples from an intermittent plume, Atmos. Environ. 18 (1984) 121–123.

[10] R.I. Sykes, D.S. Henn, Representation of velocity gradient effects in a Gaussian puff model, J. Appl. Met. 34 (1995) 2715–2723.

[11] R.I. Sykes, W.S. Lewellen, S.F. Parker, A Gaussian plume model of atmospheric dispersion based on second-order closure, J. Clim. Appl. Met. 25 (1986) 322–331.

[12] R.I. Sykes, W.S. Lewellen, S.F. Parker, D.S. Henn, A hierarchy of dynamic plume models incorporating uncertainty, Vol. 3: Second-order Closure Integrated Model Plume (SCIMP), EPRI, EPRI EA-6095 Vol. 3, Project 1616-28, 1988.

[13] R.I. Sykes, S.F. Parker, D.S. Henn, W.S. Lewellen, Numerical simulation of ANATEX tracer data using a turbulence closure model for long-range dispersion, J. Appl. Met. 32 (1993) 929–947.

[14] J.C. Weil, Plume rise, in: A. Venkatram, J.C. Wyngaard (Eds.), Lectures on Air Pollution Modeling, Am. Met. Soc., Boston, 1988, pp. 119–166.

[15] H.W.M. Witlox, The HEGADAS model for ground-level heavy-gas dispersion: I. Steady-state model, Atmos. Environ. 28 (1994) 2917–2932.